LAWRENCE
LIVERMORE
NATIONAL
LABORATORY

LLNL-PROC-812421

A Transported Livengood-Wu Integral Model for Knock Prediction in CFD Simulation

Z. Yue, C. Xu, S. Som, C. S. Sluder, K. D. Edwards, R. A. Whitesides, M. J. McNenly

July 13, 2020

Internal Combustion Engine Division Fall Technical Conference
Denver, CO, United States
November 1, 2020 through November 4, 0202

Disclaimer

A TRANSPORTED LIVENGOOD-WU INTEGRAL MODEL FOR KNOCK PREDICTION IN CFD SIMULATION

Zongyu Yue
Tianjin University and Argonne National Laboratory
Tianjin, China
Corresponding author: zongyuyue@tju.edu.cn

Chao Xu, Sibendu Som
Argonne National Laboratory
Lemont, IL

C. Scott Sluder, K. Dean Edwards
Oak Ridge National Laboratory
Knoxville, TN

Russell Whitesides, Matthew J. Mcnenly
Lawrence Livermore National Laboratory
Livermore, CA

Abstract

This work describes the development of a transported Livengood-Wu (L-W) integral model for computational fluid dynamics (CFD) simulation to predict auto-ignition and engine knock tendency. The currently employed L-W integral model considers both single-stage and two-stage ignition processes, thus can be generally applied to different fuels such as paraffin, olefin, aromatics and alcohol. The model implementation is first validated in simulations of homogeneous charge compression ignition combustion for three different fuels, showing good accuracy in prediction of auto-ignition timing for fuels with either single-stage or two-stage ignition characteristics. Then, the L-W integral model is coupled with G-equation model to indicate end-gas auto-ignition and knock tendency in CFD simulations of a direct-injection spark-ignition engine. This modeling approach is about 10 times more efficient than the ones that based on detailed chemistry calculation and pressure oscillation analysis. Two fuels with same Research Octane Number (RON) but different octane sensitivity are studied, namely Co-Optima Alkylate and Co-Optima E30. Feed-forward neural network model in conjunction with multi-variable minimization technique is used to generate fuel surrogates with targets of matched RON, octane sensitivity and ethanol content. The CFD model is validated against experimental data in terms of pressure traces and heat release rate for both fuels under a wide range of operating conditions. The knock tendency—indicated by the fuel energy contained in the auto-ignited region—of the two fuels at different load conditions correlates well with the experimental results and the fuel octane sensitivity, implying the current knock modeling approach can capture the octane sensitivity effect and can be applied to further investigation on composition of octane sensitivity.

Keywords: Knock; Livengood-Wu integral; Octane sensitivity; CFD; two-stage ignition

Nomenclature

γ	Change of T or P during LTHR
Γ	Dilution rate
τ	Ignition delay
ϕ	Equivalence ratio
AHRR	Apparent heat release rate
AI	Auto-ignited
aTDC	After top dead center
CFD	computational fluid dynamics
E	Fuel energy

FMF	Fuel mass fraction
gIMEP	gross indicated mean effective pressure
HoV	Heat of vaporization
I	L-W integral
KLSA	Knock-limited spark advance
LHV	Lower heating value
L-W	Livengood-Wu
LTHR	Low temperature heat release
MON	Motor octane number
NTC	Negative temperature coefficient
P	Pressure
PRF	Primary reference fuel
RON	Research octane number
S	Octane sensitivity
SI	Spark-ignition
T	Temperature

Introduction

Motor gasoline is expected to continuously dominate the U.S. transportation market in the near future [1]. Further improvement in the thermal efficiency of gasoline engines is therefore critical to reduce total energy consumption and CO_2 emissions. Engine knock is an abnormal combustion phenomenon typically observed in gasoline spark-ignition (SI) engines, and is caused by auto-ignition of unburnt mixture in the end-gas ahead of the propagating flame and can sometimes lead to severe damage of the engine components. Knock remains one of the major barriers to improving SI engine efficiency since a delayed spark timing or reduced compression ratio is usually required at knock-limited condition to avoid auto-ignition, but with an efficiency penalty.

Fuel composition and properties can significantly affect knock tendency. Research Octane Number (RON) [2] and Motor Octane Number (MON) [3] are currently the standard rating methods for knock resistance of fuels in SI engines. A fuel is rated by comparing its knock-limited compression ratio in a Cooperative Fuel Research (CFR) engine with primary reference fuel (PRF) blend in the RON and MON testing conditions, respectively. A practical fuel generally has different values for RON and MON, and their difference is referred to as octane sensitivity (*S*). The origin of *S* has been studied from both chemical and thermal aspects. The chemical component of *S* is mainly attributable to the fact that low-*S* fuels (e.g., paraffin) typically exhibit two-stage ignition and negative temperature coefficient (NTC) behaviors, which makes the auto-ignition process less sensitive to the unburnt gas temperature, while high-*S* fuels (e.g., olefins, aromatics and ethanol) are more sensitive to the unburnt gas temperature due to the lack of NTC behavior [4]. On the other hand, fuel heat of vaporization (HoV) has been considered as a potential thermal component of *S* since the intake temperature in the RON test is impacted by fuel evaporation cooling while the intake temperature in the MON test is not [5]. The proportion of chemical and thermal components was approximated by comparing RON and modified RON (with fuel cooling effect eliminated) for gasoline-ethanol blends, showing that the thermal component becomes important only when ethanol content is higher than 30% by volume [5][6]. Nonetheless, to better understand the origin of *S*, the chemical and thermal components such as auto-ignition delay, laminar flame speed and HoV, etc., require further investigation to quantify their contribution, which is difficult to achieve in experimental studies since the properties of real fuels are generically co-variant, while numerical approaches can be promising solutions, provided an accurate knock modeling approach that incorporates fuel effects is available.

Computational Fluid Dynamics (CFD) has become an effective tool for understanding the knock phenomenon. Liang et al. [7] coupled the level-set G-equation combustion model [8] with detailed chemical kinetics to simulate knocking combustion in a boosted direct-injection SI (DISI) engine. This hybrid method has been widely adopted since then, and approaches like maximum amplitude

pressure oscillation (MAPO) analysis [9][10], intermediate species analysis [11] and detonation theory analysis [12] can be applied to the CFD results to determine knock onset or knock tendency. This hybrid approach typically employs detailed chemical mechanisms to accurately predict auto-ignition. The large number of species in a detailed mechanism leads to increased computational expense, limiting its application for parametric study and design optimization, especially in knock study wherein a spark timing sweep is usually necessary to identify knock-limited spark advance (KLSA). In addition, a small Mach Courant–Friedrichs–Lewy (CFL) number less than unity and consequently a small CFD time-step are required for pressure oscillation analysis, which further makes it computationally expensive to accurately predict knock in CFD simulation.

Recently, a transported Livengood-Wu (L-W) integral model has been proposed by the authors [13], which introduces the L-W integral into CFD for indication of end-gas auto-ignition. The L-W integral is transported in the CFD domain as a passive species, and the global reaction rate is tabulated from chemical kinetic calculations. A criterion calibrated against experiment was developed to provide accurate prediction of KLSA at multiple operating conditions. This approach achieves about 10 times faster simulation run time compared to the ones that solve detailed chemical kinetics, since detailed kinetics calculations and transport of hundreds of species are avoided, and simulations can run with a large Mach CFL of 50. In this previous work, a single-stage L-W integral model was used, assuming that the global reaction rate only depends on the unburnt thermodynamic condition and can be approximated by the reciprocal of total ignition delay. While this single-stage approach was demonstrated successful in knock prediction for a gasoline fuel that has limited low-temperature heat release (LTHR) under boosted SI conditions, it is worthy to examine how well this approach can be generalized to other fuels that exhibit evident two-stage ignition behavior.

In the current work, the L-W knock model presented in Reference [13] is further improved and extended to account for the two-stage ignition behavior by applying a staged L-W integral approach. This allows the L-W knock model to be applied to fuels with different ignition behavior and *S*, and potentially enables further numerical analysis and better understanding of the *S* origin. Commercial CFD software CONVERGE 2.4 [14] is employed for the simulations and the new model is implemented through a user defined function. Predictions of auto-ignition by both the single-stage and two-stage L-W integral approaches are compared against detailed chemistry calculation in homogeneous charge compression ignition (HCCI) simulations for three types of fuels: PRF20, Co-Optima Alkylate and Co-Optima E30 [15]. Then, the transported L-W integral model is coupled with the G-Equation model to predict knock in DISI engine simulations. The capability of capturing knock tendency for fuels with different *S* is also discussed.

Livengood-Wu integral model for auto-ignition prediction

Fuel surrogates

To enable simulations, surrogate fuels were generated for the Co-Optima Alkylate and Co-Optima E30 fuels, which were designed to have similar RONs but different *S* [15]. A three-component toluene primary reference fuel (TPRF) and a four-component TPRF-ethanol (TPRF-E) were obtained using a multi-variable minimization technique in conjunction with prediction models for RON and MON. Specifically, the difference between predicted and target RON and MON with respect to component volume fractions was minimized, subject to the constraints of the sum of the volume fractions being unity and, in the case of E30, the ethanol volume fraction being 30.59%. The details of the surrogate compositions and properties are shown in Table 1, along with properties of the real fuels.

Table 1. Fuel surrogates composition and properties compared with real values [15]. Density and HoV are at 298 K, 1 bar.

	Alkylate	E30
Real fuel properties		

Density (kg/m3)	696.8	752.7
HoV (kJ/kg)	309.40	564.70
LHV (kJ/kg)	44520	38170
RON/MON	98.0/96.6	97.4/86.6
Ethanol (%vol)	0	30.59
Surrogate composition		
iso-octane	0.90049	0.18865
n-heptane	0.03395	0.21285
Toluene	0.06556	0.28266
Ethanol	0	0.31584
Surrogate properties		
Density (kg/m3)	697.8	759.6
HoV (kJ/kg)	309.50	527.14
LHV (kJ/kg)	44418.52	38311.51
RON/MON	98.0/96.6	97.4/86.6
Ethanol (%vol)	0	30.59

The RON/MON prediction models employed were feed-forward neural networks [16] that relate the ignition chemistry from a detailed chemical kinetics model [17] and other thermophysical properties to the octane rating. Two feed-forward neural networks were created, one each for RON and MON. Both models used the same inputs and architecture – a single hidden layer with 24 nodes. The inputs included three ignition delay related quantities, simulated using the detailed chemistry model [17] in a homogenous, constant-volume reactor at 825 K and 20 bar. These were the inverse of the ignition delay time to reach 1225 K, and the derivative of the normalized ignition delay time with respect to pressure and temperature. The other neural network inputs were the enthalpy of vaporization and liquid density at 298 K, and the mole-averaged atom counts of hydrogen, carbon and oxygen. The neural network was demonstrated to have good predictive capability with root-mean-square errors (RMSE) in RON/MON of approximately 1 octane number for cross-validation data. Further details on the design, implementation, and validation of the neural network can be found in [18].

Livengood-Wu integral model

The L-W integral [19] was traditionally used to predict engine auto-ignition. The global reaction rate is approximated by the reciprocal of ignition delay at given temperature and pressure, and the temporal integration of the global reaction rate along the engine pressure-temperature trajectory indicates a progress towards auto-ignition. The mixture is considered 'auto-ignited (AI)' when this integral reaches unity. The ignition delay can be either estimated using an Arrhenius-based correlation [19] or tabulated from chemical kinetics calculation [13]. It has been pointed out that the traditional L-W integral model, which considers the ignition as a single-step process, can be problematic when applying to fuels that exhibit two-stage ignition characteristics (e.g., paraffin), and a staged integration method is required to accommodate those fuels [20]. Figure 1 shows an example of two-stage auto-ignition process in a constant volume homogeneous reactor. As can be seen, the total ignition delay, τ_{tot}, can be divided into two parts: the first-stage ignition delay, τ_1, and the second-stage ignition delay, τ_2, which are defined by the first and second temperature inflection points, respectively. After the first-

stage ignition, the temperature is increased due to LTHR, as indicated by T_{LTHR} at the minimum temperature rise rate point between τ_1 and τ_{tot}.

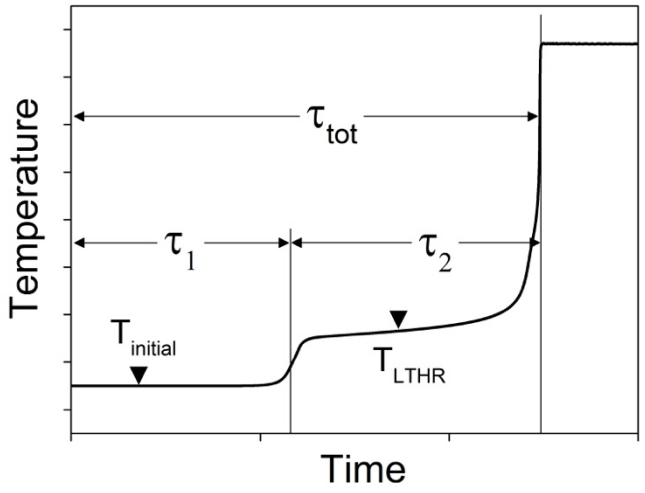

Figure 1. Illustration of a two-stage auto-ignition process.

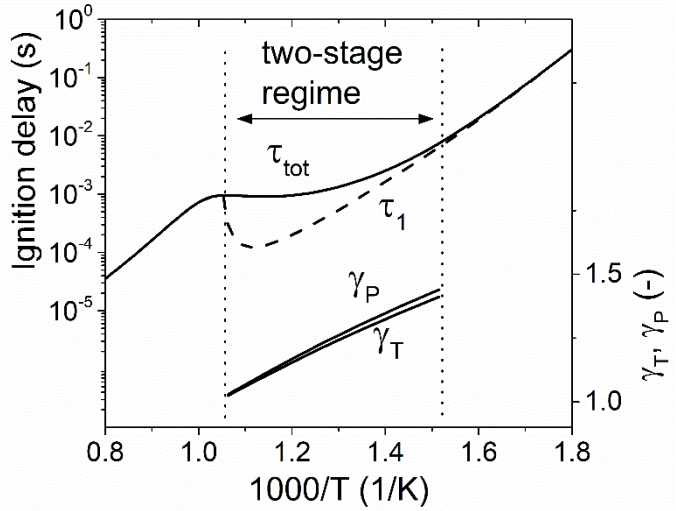

Figure 2. First-stage (τ_1) and total (τ_{tot}) ignition delay at 40 bar, 0.5 equivalence ratio for PRF20-air mixture. The ratios of pressure (γ_P) and temperature (γ_T) increases after first-stage ignition are plotted for the two-stage regime.

Figure 2 shows the constant-volume ignition delay as function of initial temperature, calculated using a reduced mechanism [21] for PRF20 and air mixture at 40 bar. τ_{tot} is shown by the solid line, while τ_1 is shown by the dashed line in the two-stage regime as bounded by the dotted lines. The difference between τ_1 and τ_{tot} is τ_2. Both temperature and pressure increase due to the LTHR after the first-stage ignition. These changes are characterized as $\gamma_T = T_{LTHR}/T_{initial}$ and $\gamma_P = P_{LTHR}/P_{initial}$.

For the single-stage ignition regime, only the total ignition delay and single-step integration need to be considered. The single-stage L-W integral, I_s, is tracked as a passive scalar and is used to indicate local progress towards auto-ignition.

$$\partial_t(\rho\tilde{I}_s) + \nabla(\rho\boldsymbol{u}\tilde{I}_s) - \nabla\cdot(\rho D_T\nabla\tilde{I}_s) = \rho\dot{\omega}_s \qquad (1)$$

$$\dot{\omega}_s = 1/\tau_{tot}(T, P, \phi, \Gamma) \qquad (2)$$

Here, $\tilde{}$ denotes the Favre-averaged mean value. The impact of sub-grid turbulent fluctuation on end-gas auto-ignition was found to be marginal for the studied engine cases [13] and is neglected in this work. The chemical source term $\dot{\omega}_s$ is determined as the reciprocal of ignition delay τ_{tot} based on local temperature (T), pressure (P), equivalence ratio (ϕ) and dilution rate (Γ).

For the two-stage ignition regime, a staged integration method is applied. Two L-W integrals, I_1 and I_2, are considered, indicating local progress towards the first-stage and second-stage ignition, respectively. These two integrals are transported similarly to I_s as in Eq. (1) but with different source terms as shown in Eq. (3) and (4), respectively. The source term for second integral I_2, $\dot{\omega}_2$, remains 0 until the local I_1 reaches unity. It should be noted that τ_2 is a function of local thermodynamic state after the first-stage ignition (i.e., $\gamma_T T$ and $\gamma_P P$), instead of local non-reacting condition (i.e., T and P) which does not account for LTHR since the auto-ignition heat release is not coupled with the energy equation. Here, γ_T and γ_P are also transported in the computational domain, both initialized at a value of 1 and assigned the value as function of local conditions only at the instant when first-ignition occurs.

$$\dot{\omega}_1 = 1/\tau_1(T, P, \phi, \Gamma) \quad (3)$$

$$\dot{\omega}_2 = \begin{cases} 0 & when\ I_1 < 1 \\ 1/\tau_2(\gamma_T T, \gamma_P P, \phi, \Gamma) & when\ I_1 \geq 1 \end{cases} \quad (4)$$

All the L-W integral related parameters, τ_1, τ_2. τ_{tot}, γ_T and γ_P, are calculated for each fuel using the CONVERGE 0D solver and tabulated *a priori* in the dimensions of T (from 500 to 1500 K with 10 K step), P (from 5 to 70 bar with 5 bar step), ϕ (from 0.4 to 2.0 with 0.1 step), Γ (from 0 to 0.2 with 0.05 step). The reduced TPRF-E mechanism is employed, which has been validated for engine combustion application [21][22]. For the single-stage ignition regime, the values of γ_T and γ_P are 1, and the values of τ_1 and τ_2 are assigned both equal to τ_{tot}. As a result, the staged integration would over-predict the ignition delay when applied in the single-stage regime as will be shown in section 2.3.

In order to ensure that the L-W integral model can be accurately applied to both single-stage and two-stage ignition regimes, the single-stage and two-stage L-W integration approaches are solved simultaneously and independently in the current CFD implementation, and auto-ignition is predicted when any of I_s and I_2 reaches unity. In other words, while the two-stage L-W model would fail in the single-stage ignition regime, the single-stage L-W result can guarantee accurate auto-ignition prediction, and vice versa for the two-stage ignition regime.

Validation in 0D HCCI

The implementation of L-W integral model is validated against detailed chemical kinetics calculation in 0D HCCI combustion with a compression ratio of 16, as shown in Figure 3, Figure 4 and Figure 5 for PRF20, alkylate and E30, respectively. At each condition, the results of single-stage (green dash-dot lines) and two-stage L-W integrals (blue dashed and red dotted lines) are obtained from the same simulation run with detailed chemistry solver turned off. The temperature profile (black solid lines) is predicted by the detailed chemistry from a separate simulation run with the same initial conditions. The simulations start at -143° after top dead center (aTDC) with the initial conditions as shown in the figures, representing typical pressure-temperature trajectories in SI engines.

For PRF20 at initial condition of 350 K and 1 bar, 0.5 equivalence ratio and 1000 rpm as seen in Figure 3 (a), the first-stage ignition occurs around -22 aTDC and the second-stage integral starts to rise immediately, while the single-stage integral continuously grows during the ignition process. The ignition timings predicted by the single-stage and two-stage L-W integrals are very close, and both agree well with the detailed chemistry results. Similarly, both L-W integration approaches provide satisfying prediction of auto-ignition when the initial pressure is increased to 2 bar. However, when the initial temperature is increased to 380 K, the second-stage ignition

delay is increased due to the NTC behavior as seen in the temperature profile. Consequently, difference between two L-W integral approaches becomes evident. Two predicted ignition timings further deviate as the engine speed is increased to 2000 rpm in Figure 3 (d), and the single-stage L-W approach fails in predicting ignition timing.

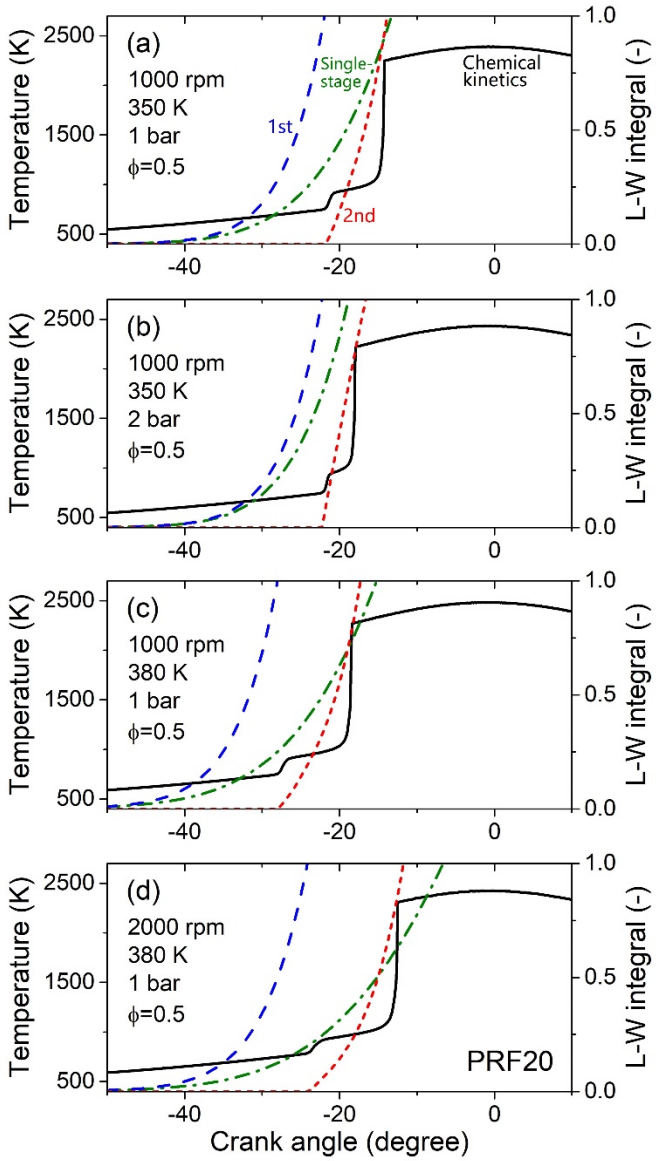

Figure 3. Comparison of single-stage (green dash-dot) and two-stage (first-stage: blue dashed; second-stage: red dotted) L-W integrals with in-cylinder temperatures from detailed kinetics (black solid) in 0D HCCI with PRF20.

For alkylate fuel, a stoichiometric condition is selected to be relevant to typical SI engine conditions. Similar observations from the PRF20 cases are also found for the alkylate cases in Figure 4. The single-stage approach works as well as the two-stage integration approach at initial temperature of 350 K, but at initial temperature of 380 K, only the two-stage approach is accurate while the single-stage approach over-predicts the ignition timing. This is because the alkylate fuel and its surrogate mostly consists of iso-paraffin, although the temperature increase during the second-stage ignition is not as significant as for PRF20. On the other hand, the ignition for E30 is a single-stage process as seen in the temperature profile in Figure 5, and the single-stage L-W model is sufficient to accurately

predict the ignition timing. The profile of first-stage integral overlaps with the single-stage integral, while the second-stage integral fails to predict ignition accurately.

It is seen that the two-stage L-W integral model is generally favorable for paraffin fuels with two-stage ignition characteristics, especially for the higher temperature end of the two-stage regime that has longer second-stage ignition delay as seen in Figure 1. However, for the lower temperature end of the two-stage regime, wherein the second-stage ignition delay is shorter, the single-stage L-W model works satisfactorily as seen in the cases of PRF20 and alkylate with initial temperature of 350K in Figure 3 and Figure 4. In addition, increasing pressure would also reduce the LTHR and make the two L-W integral approaches work equivalently.

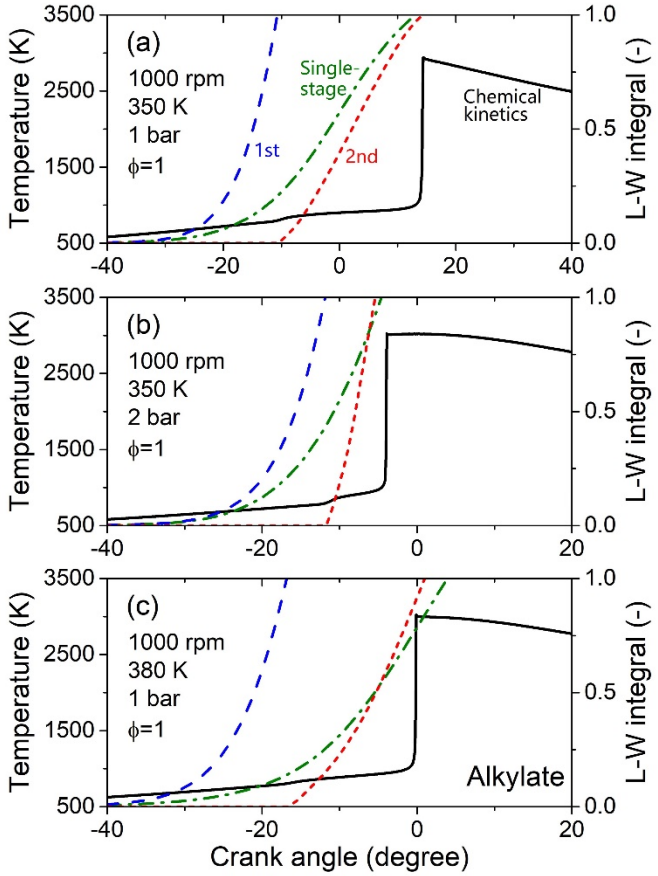

Figure 4. Comparison of single-stage (green dash-dot) and two-stage (first-stage: blue dashed; second-stage: red dotted) L-W integrals with in-cylinder temperatures from detailed kinetics (black solid) in 0D HCCI with alkylate.

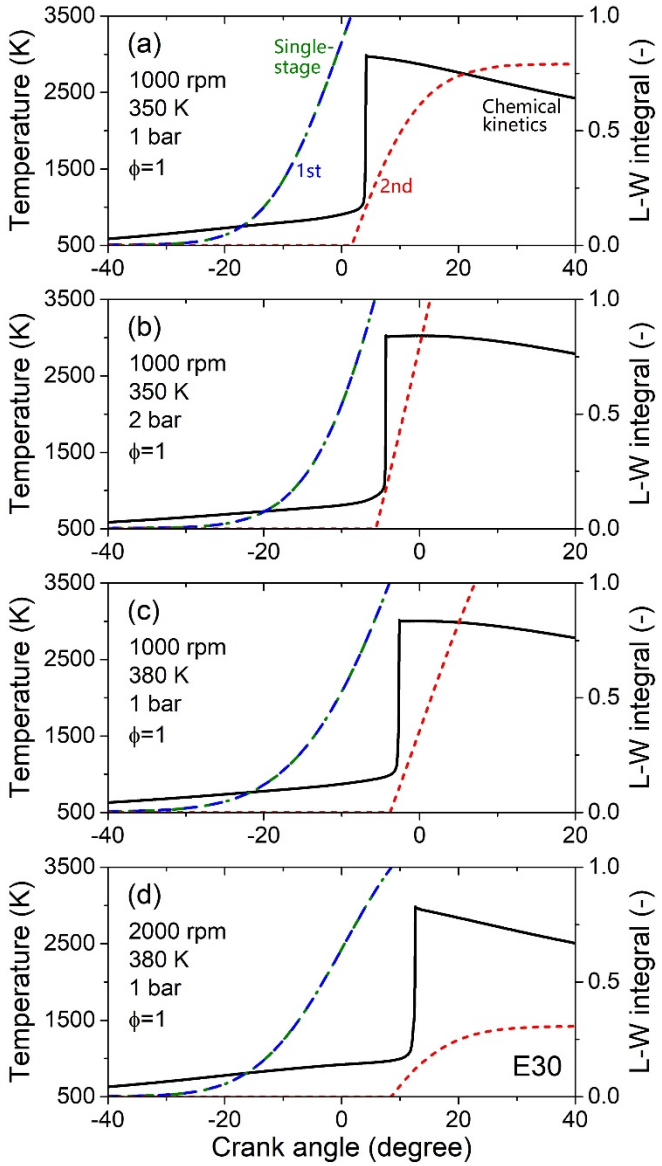

Figure 5. Comparison of single-stage (green dash-dot) and two-stage (first-stage: blue dashed; second-stage: red dotted) L-W integrals with in-cylinder temperatures from detailed kinetics (black solid) in 0D HCCI with E30.

Application of Livengood-*Wu integral model for knock prediction*

DISI engine model

The modeled engine in this section is a 1.6-L Ford EcoBoost engine operated with the production turbocharger and direct-injection fueling system at Oak Ridge National Laboratory (ORNL). The engine specifications are summarized in Table 2. The engine geometry for CFD simulation is shown in Figure 6. Figure 7 summarizes the engine operating and boundary conditions measured from experiments for both alkylate and E30 fuels, which covers a wide range of conditions from throttled, low-load to boosted, high-load, at stoichiometric air-fuel ratio and 2000 rpm engine speed.

A modified cut-cell Cartesian grid generation method is employed to automatically generate the computational grid at runtime in CONVERGE. The base mesh size was set to be 2 mm, with 1 mm refinement applied to the in-cylinder region, 0.5 mm boundary

refinement applied on the walls and 0.25 mm mesh refinement applied to the spark region. The total cell count varies during a full engine cycle and peaks at 1.2 million near bottom dead center. The turbulent flow was modeled by a generalized re-normalized group k-ε model [23] with a temperature wall function [24] employed for the wall heat transfer. The Peng-Robinson equation of state [25] was used to correctly describe pressure-volume-temperature relationship during compression [26]. A Lagrangian model that consists of the hybrid Kelvin-Helmholtz Rayleigh-Taylor breakup model [27], No Time Counter collision model [28] and Frossling correlation [29] was used to account for the spray atomization process of droplet breakup, collision and vaporization.

Table 2. Engine specifications for experiments at ORNL.

Engine	Ford 1.6 L EcoBoost
Bore * stroke	79.0 mm * 81.3 mm
Conrod length	133 mm
Compression ratio	10.1 : 1
Fueling system	Center-mounted, direct injection, production injector
Injection pressure	130 bar
Start of injection	-300° aTDC
Fuel	Co-Optima Alkylate, Co-Optima E30

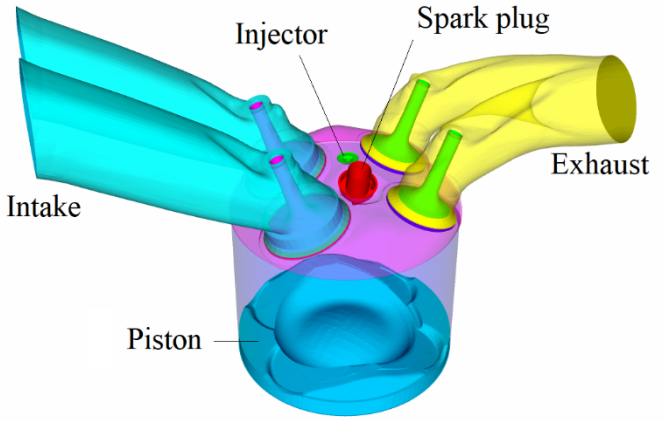

Figure 6. Engine geometry used for simulations.

Turbulent premixed combustion was captured by the level set G-equation model [8]. According to the flamelet modeling theory of Peters [8], under both the corrugated flamelet and thin reaction zone regimes, the inner reactive-diffusive layer of the flame can be modeled as an interface with infinitesimal thickness, which is tracked by solving the transport equations for a scalar G and its variance G''^2 [14]:

$$\partial_t(\rho\tilde{G}) + \nabla(\rho\boldsymbol{u}\tilde{G}) = -\rho D_t'\tilde{\kappa}|\nabla\tilde{G}| + \rho_u s_T|\nabla\tilde{G}| \qquad (5)$$

$$\partial_t(\rho\widetilde{G''^2}) + \nabla(\rho\boldsymbol{u}\widetilde{G''^2}) = \nabla\cdot(\rho D_T\nabla\widetilde{G''^2}) + 2\rho D_T(\nabla\tilde{G})^2 - c_s\rho\widetilde{G''^2}\,\varepsilon/k \qquad (6)$$

Here, ρ and ρ_u are the burnt and unburnt gas density, respectively. D_T and D_T' are the turbulent diffusivities [14]. κ is the mean flame front curvature. k and ε are the turbulent kinetic energy and its dissipation rate, respectively. s_T is the turbulent flame speed, and can be calculated using a turbulent burning velocity relationship for RANS turbulence models [8],

$$s_T = s_L + u'\{-a_4 b_3^2/2b_1 Da + [(a_4 b_3^2/2b_1 Da)^2 + a_4 b_3^2 Da]^{0.5}\} \quad (7)$$

where u' is the turbulent velocity fluctuation, s_L is the laminar flame speed, and Da is the Damköhler number. a_4, b_1 and b_3 are model constants and are set to be 0.78, 2.5 and 1, respectively. $G(x,t)$ is the distance function relative to the mean flame front, wherein $G < 0$ indicates unburnt region and $G > 0$ indicates burnt region. The spark-ignition process was modeled by directly sourcing G in a spherical volume with a radius of 0.5 mm located at the center of the spark plug gap. Laminar flame speed was calculated and tabulated *a priori* [9] using CONVERGE 1D solver with the same reduced mechanism used for ignition delay calculations. The L-W integral model was implemented in conjunction with the G-equation model and was applied to the unburnt region ($G < 0$) to predict end-gas auto-ignition.

The model setup and parameters were not changed for all the cases and fuels. Only intake/exhaust boundary conditions and spark timings were specified based on experimental measurement as shown in Figure 7. Eight consecutive open-cycles were simulated for each set of condition to achieve convergence in the cycle-averaged results [13] that are used for analysis henceforth. Each cycle runs for 8 hours on 72 cores with the current model. In contrast, the run time can be 10 times as long when the chemical kinetics is solved and a pressure-based knock analysis is applied [9]. Figure 8 and Figure 9 present the validation of the DISI engine model at all conditions for alkylate and E30 fuels. Cylinder pressure traces and apparent heat release rate (AHRR) are compared against experimental measurement and the overall match is good considering the wide range of conditions. The relative error in prediction of net indicated mean effective pressure is less than 8% and the error in CA10 and CA50 is less than 4 crank angle degree. The current model is shown able to accurately predict the trend in flame propagation corresponding to the varied operating condition, giving confidence to applying this model for predicting knock.

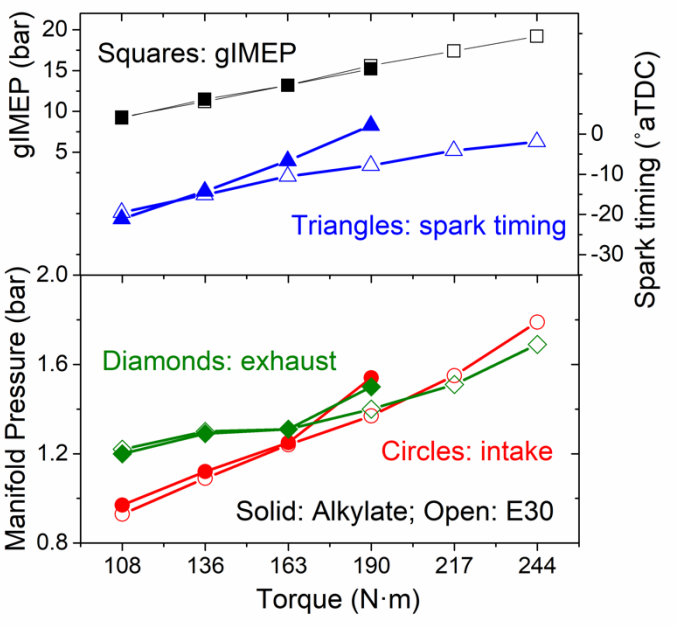

Figure 7. Engine experimental conditions for alkylate and E30.

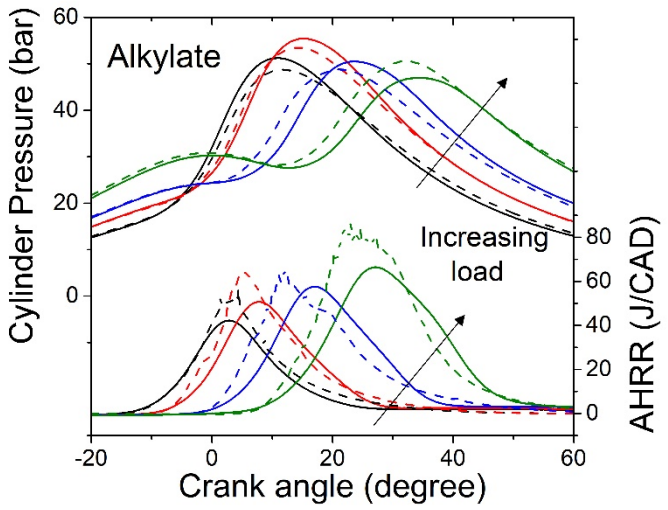

Figure 8. Validations of DISI engine simulations with Co-Optima Alkylate under 4 load conditions. Solid lines: experimental data averaged from 300-cycle measurements. Dashed: CFD predictions averaged from 8-cycle runs.

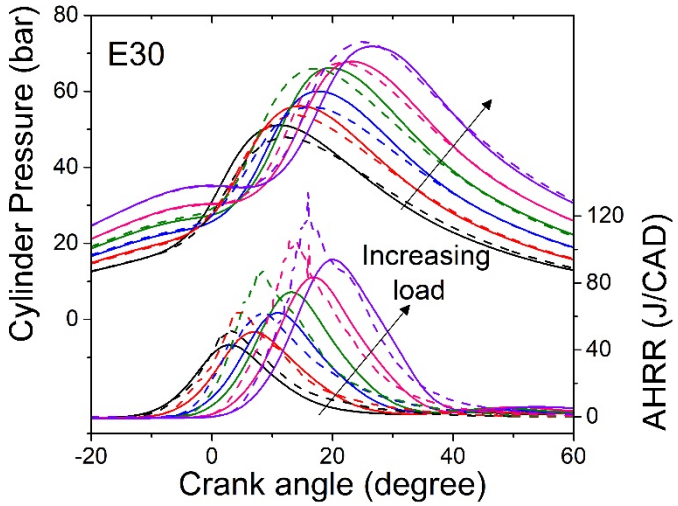

Figure 9. Validations of DISI engine simulations with Co-Optima E30 under 6 load conditions. Solid lines: experimental data averaged from 300-cycle measurements. Dashed: CFD predictions averaged from 8-cycle runs.

Effects of octane sensitivity on knock tendency

Three parameters derived from L-W integral model can be potentially employed to indicate knock. Vol_{AI} is the total volume of cells that auto-ignite as predicted by the L-W integral. FMF_{AI} and E_{AI} are the fuel mass fraction and fuel energy contained in that AI volume. Figure 10 shows the predicted profiles of these three parameters for alkylate at 136 N·m condition with spark timing swept from -12.23 to -18.23° aTDC. The increase in these profiles represent the accumulation of AI cells as the end-gas is continuously compressed by the propagating flame. The profile declines after reaching its peak since the end-gas is consumed by the flame. A bi-modal profile is seen at retarded spark timing, which is caused by the non-uniform spatial growth of the flame. It was shown in our previous study [13] that the peak values of Vol_{AI} correlates well with knock tendency and can be used to determine knock onset and KLSA in a boosted SI engine with alkylate fuel under stoichiometric operation, and the use of FMF_{AI} and E_{AI} can potentially generalize this metric to other fuels and conditions, e.g., stratified or lean operation. As seen in Figure 10, the peak value of each profile increases when the spark timing is advanced, indicating an increased knock tendency. The trends and shapes in Vol_{AI}, FMF_{AI} and E_{AI}

profiles are similar since the fuel is almost homogeneously distributed in the current study. Henceforth, E_{AI} is used to compare knock tendency between alkylate and E30 since it accounts for the differences in stoichiometric air-fuel ratios and lower heating values of different fuels.

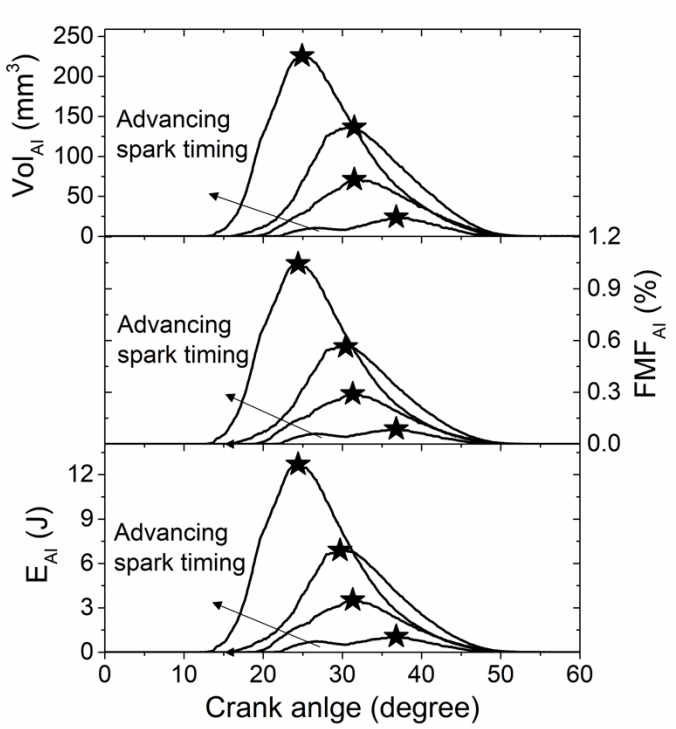

Figure 10. Profiles of AI volume, AI FMF and AI energy for alkylate at 136 N·m condition. Spark timing varied from -12.23 to -18.23° aTDC with 2 crank angle degree increment. Symbols mark the peak points.

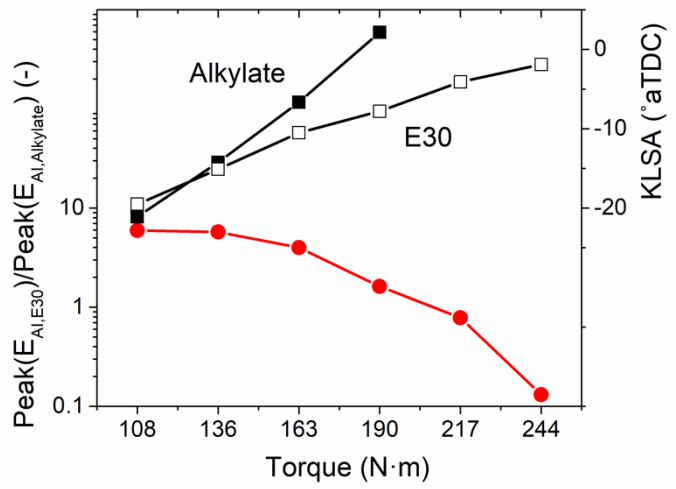

Figure 11. Peak AI energy ratio (circle lines) of E30 and alkylate, and experimental KLSA (square lines) for both fuels.

The ratio of peak values in E_{AI} between E30 and alkylate is shown in Figure 11 for different load conditions. Here, the alkylate results were simulated using the same intake/exhaust conditions and spark timings from E30 cases to ensure a fair comparison of fuels, and the injected mass of alkylate was adjusted to maintain a stoichiometric mixture. The ratio of peak values in E_{AI} is about 6 at 108 N·m condition, indicating a higher knock tendency for E30 than alkylate. As the operating load increases, the ratio declines

monotonically to less than unity, suggesting that the more knock-prone fuel changes from E30 to alkylate. Also presented in Figure 11 is the experimental KLSA, which was experimentally measured as the crank angle before a significant increase in the knock meter reading was observed when gradually advancing the spark timing. The different slopes in KLSA for alkylate and E30 is related to the different *S* of the two fuels. As the intake pressure increases with increasing load, the operating condition is shifted towards the beyond-RON condition. Consequently, the E30 with higher *S* is more knock-resistant at these beyond-RON conditions and allows more advanced spark timing compared to alkylate. The two KLSA profiles cross around the 136 N·m since that condition is close to the RON test condition and both fuels have similar RONs. The simulation result shows the location of switch in knock propensity (the E_{AI} ratio equals unity) occurs around 190 N·m. This deviation between experiment and simulation could be caused by a number of reasons, such as the inaccuracies in the prediction of main combustion events, surrogate formula, as well as the inconsistencies between the detailed mechanism that used to formulate surrogate and the reduced mechanism that was employed for L-W integral model tabulation, which can be potentially improved in future work. Nonetheless, the CFD prediction captures the trend in knock tendency of two fuels with different *S*, suggesting the current modeling framework coupling G-equation model with L-W integral model can incorporate the effect of *S* on knock tendency and can be applied to further investigate the origin of *S*. A detailed analysis is possible with this numerical approach to decompose and quantify the impact of different fuel properties, such as ignition delay, flame speed and HoV, on the measured *S*.

Summary and conclusions

In this study, a transported L-W integral model was developed and implemented in CFD simulation for engine knock study. The current framework is 10 times more efficient in computational run time compared to an approach applies chemical kinetics calculation and pressure oscillation analysis [9]. This model can be applied to auto-ignition prediction for fuels with either single-stage or two-stage ignition characteristics by solving both the single-stage and two-stage L-W integrals simultaneously. The L-W integral model was validated against detailed chemical kinetics in HCCI combustion at several conditions for three different fuels, namely PRF20, Co-Optima Alkylate and Co-Optima E30. The TPRF-E surrogates for the Co-Optima fuels were generated using multi-variable minimization method and neural network model by matching the RON, MON and ethanol content. The two-stage integration approach was shown to perform better than the traditional single-stage approach in prediction of auto-ignition in HCCI combustion for paraffin fuels, especially at high initial temperature (380 K), but the difference between two approaches is marginal at low initial temperature (350 K) and high initial pressure (2 bar), while the two-stage approach fails for fuels that only have single-stage ignition process, i.e. Co-Optima E30. Therefore, the current implementation combining both single-stage and two-stage integration approaches is justified to extend the L-W integral model for a wide range of fuels that relevant to engines and to provide accurate predictions of auto-ignition as presented in the HCCI validations. The L-W integral model was then applied to DISI engine combustion to predict end-gas auto-ignition and knock tendency for Co-Optima alkylate and Co-Optima E30, two fuels with similar RON but different *S*. The predictions of SI combustion agree well with the experiment for a wide range of operating conditions without case-by-case model adjustment. The effect of *S* on knock tendency from experiment was also captured by the current model as indicated by the comparison of the peak auto-ignited fuel energy of two fuels, wherein the E30 fuel with higher *S* is more knock-prone at low load and is more knock-resistant at high load compared to the alkylate. While further model improvement for quantitative analysis is necessary in the future work, the current results suggest the potential of applying this L-W integral knock model to investigating fuel effects on engine knock, e.g., the origin of *S*.

Acknowledgements

UChicago Argonne, LLC, operator of Argonne National Laboratory ("Argonne"), a U.S. Department of Energy (DOE) Office of Science laboratory, is operated under Contract No. DE- AC02-06CH11357. The U.S. Government retains for itself, and others acting on its behalf, a paid-up nonexclusive, irrevocable worldwide license in said article to reproduce, prepare derivative works, distribute copies to the public, and perform publicly and display publicly, by or on behalf of the Government. This research was partially funded by DOE's Office of Vehicle Technologies, Office of Energy Efficiency and Renewable Energy under Contract No. DE-AC02-06CH11357. The authors wish to thank Gurpreet Singh, Kevin Stork, and Michael Weismiller, program managers at DOE, for their support. This research was conducted as part of the Co-Optimization of Fuels & Engines (Co-Optima) project sponsored by the U.S. DOE Office of Energy Efficiency and Renewable Energy, Bioenergy Technologies and Vehicle Technologies Offices. The authors would like to acknowledge the Laboratory Computing Resource Center (LCRC) at Argonne National Laboratory (ANL) for computing resource on the Bebop cluster that were used in this research.

References

[1] https://www.eia.gov/totalenergy/data/monthly/

[2] ASTM International, 2012, "Standard Test Method for Research Octane Number of Spark-Ignition Engine Fuel," ASTM International, West Conshohocken, PA. Standard No. ASTM D2699-12.

[3] ASTM International, 2016, "Standard Test Method for Motor Octane Number of Spark-Ignition Engine Fuel," ASTM International, West Conshohocken, PA. Standard No. D2700-16.

[4] Leppard, W. R., 1990, "The chemical origin of fuel octane sensitivity," SAE Technical Paper No. 902137.

[5] Sluder, C. S., Szybist, J. P., McCormick, R. L., Ratcliff, M. A., and Zigler, B. T., 2016, "Exploring the Relationship Between Octane Sensitivity and Heat-of-Vaporization," SAE Int. J. Fuels Lubr., 9(1), pp. 80-90.

[6] Foong, T. M., Morganti, K. J., Brear, M. J., da Silva, G., Yang, Y., and Dryer, F. L., 2013, "The Effect of Charge Cooling on the RON of Ethanol/Gasoline Blends," SAE Int. J. Fuels Lubr., 6(1), pp. 34-43.

[7] Liang, L., Reitz, R. D., Iyer, C., and Yi, J., 2007, "Modeling Knock in Spark-Ignition Engines Using a G-equation Combustion Model Incorporating Detailed Chemical Kinetics," SAE Technical Paper No. 2007-01-0165.

[8] Peters, N., 2000, Turbulent Combustion, Cambridge University Press, Cambridge, U.K.

[9] Yue, Z., Edwards, K. D., Sluder, C. S., and Som, S., 2019, "Prediction of Cyclic Variability and Knock-Limited Spark Advance in a Spark-Ignition Engine," ASME J. Energy Resour. Technol., 141, pp. 102201.

[10] Pal, P., Wu, Y., Lu, T., Som, S., See, Y. C., and Le Moine, A., 2018, "Multidimensional Numerical Simulations of Knocking Combustion in a Cooperative Fuel Research Engine," ASME J. Energy Resour. Technol., 140(10), pp. 102205.

[11] Shao, J., and Rutland, C. J., 2014, "Modeling Investigation of Different Methods to Suppress Engine Knock on a Small Spark Ignition Engine," J. Eng. Gas Turb. Power, 37, pp. 61506.

[12] Netzer, C., Seidel, L., Pasternak, M., Lehtiniemi, H., Perlman, C., Ravet, F., and Mauss, F., 2018, "Three-dimensional computational fluid dynamics engine knock prediction and evaluation based on detailed chemistry and detonation theory," Int. J. Eng. Res., 19, pp. 33-44.

[13] Yue, Z., and Som, S., 2019, "Fuel Property Effects on Knock Propensity and Thermal Efficiency in a Direct-Injection Spark-Ignition Engine," Appl. Energy, DOI: 10.1016/j.apenergy.2019.114221.

[14] CONVERGE 2.4 Theory Manual, Convergent Science Inc., Middleton, WI, 2018.

[15] Fouts, L., Fioroni, G. M., Christensen, E., et al., 2018, Properties of Co-Optima Core Research Gasolines. Report No. NREL/TP-5400-71341, National Renewable Energy Laboratory.

[16] <https://scikit-learn.org/stable/modules/neural_networks_supervised.html>

[17] Mehl, M., Wagnon, S., Tsang, K., et al., 2017, "A comprehensive detailed kinetic mechanism for the simulation of transportation fuels," 10th US Natl. Combust. Meeting.

[18] Pal, P., Kalvakala, K., Wu, Y., et al., 2019, "Numerical Investigation of a Central Fuel Property Hypothesis under Boosted Spark-Ignition Conditions," ASME ICEF, ICEF2019-7284.

[19] Livengood, J. C., and Wu, P. C., 1955, "Correlation of autoignition phenomena in internal combustion engines and rapid compression machines," Symp. (Int.) Combust., 5, pp. 347-356.

[20] Tao, M., Han, D., and Zhao, P., 2017, "An Alternative Approach to Accommodate Detailed Ignition Chemistry in Combustion Simulation," Comb. Flame, 176, pp. 400-408.

[21] Wang, H., Yao, M., Yue, Z., Jia, M., and Reitz, R. D., 2015, "A reduced toluene reference fuel chemical kinetic mechanism for combustion and polycyclic-aromatic hydrocarbon predictions," Combust. Flame, 162, pp. 2390-2404.

[22] Ren, S., Kokjohn, S. L., Wang, Z., Liu, H., Wang, B., and Wang, J., 2017, "A multi-component wide distillation fuel (covering gasoline, jet fuel and diesel fuel) mechanism for combustion and PAH prediction," Fuel, 208, pp. 447-468.

[23] Wang, B.-L., Miles, P. C., Reitz, R. D., Han, Z., and Petersen, B., 2011, "Assessment of RNG Turbulence Modeling and the Development of a Generalized RNG Closure Model," SAE Technical Paper No. 2011-01-0829.

[24] Han, Z., and Reitz, R. D., 1997, "A temperature wall function formulation for variable-density turbulent flows with application to engine convective heat transfer modeling," Int. J. Heat Mass Transfer, 40, pp. 613-625.

[25] Peng, D.-Y., and Robinson, D. B., 1976, "A new two-constant equation of state," Ind. Eng. Chem. Fund., 15, pp. 59–64.

[26] Yue, Z., Hessel, R., and Reitz, R. D., 2018, "Investigation of real gas effects on combustion and emissions in internal combustion engines and implications for development of chemical kinetics mechanisms," Int. J. Eng. Res., 19(3), pp. 269–281.

[27] Beale, J. C., and Reitz, R. D., 1999, "Modeling spray atomization with the Kelvin-Helmholtz/Rayleigh-Taylor hybrid model," Atomization Spray, 9, pp. 623-650.

[28] Schmidt, D. P., and Rutland, C. J., 2000, "A New Droplet Collision Algorithm," J. Comput. Phys., 164, pp. 62-80.

[29] Amsden, A. A., 1997, KIVA-3V: A Block Structured KIVA Program for Engines with Vertical or Canted Valves, Report No. LA-13313-MS, Los Alamos National Laboratory.